12th IFAC International Symposium on
Advanced Control of Chemical Processes
July 14-17, 2024. Toronto, Canada

Model-based design of the temperature controller of a shrink tunnel

Davide Previtali * **Leandro Pitturelli** * **Antonio Ferramosca** *
Fabio Previdi *

* *Department of Management, Information and Production Engineering, University of Bergamo, Via G. Marconi 5, 24044 Dalmine (BG), Italy (e-mail: davide.previtali@unibg.it)*

Abstract: Shrink tunnels are machines composed of an industrial oven and a conveyor belt; they are widely used in manufacturing applications for polymeric packaging. Manufacturing products are wrapped in a thin plastic film and inserted into the oven via the conveyor belt. The heat shrinks the plastic around the products, creating the pack. This paper presents a model-based temperature control architecture that tackles numerous goals: setpoint tracking in the presence of manual-automatic transitions, demanding disturbance rejection requirements, energy saving, and actuator limitations. The performances of the control architecture are experimentally validated on a workbench, highlighting its effectiveness in satisfying the specifications.

Keywords: Temperature control, Black-box modelling, MIMO systems, Centralized control, PID control, Shrink tunnel.

1. INTRODUCTION

Temperature control is a vast and diverse thermal engineering field, covering applications that range from small kitchen appliances, such as convection ovens (Ryckaert et al. (1999)), to large Heating, Ventilation and Air Conditioning (HVAC) systems in buildings (Afroz et al. (2018)). Other relevant applications include: industrial furnaces (Zhang et al. (2014)), heat exchangers (Vasičkaninová et al. (2011)), heat pumps (Rastegarpour et al. (2020)), and environmental chambers (He et al. (2014)).

Designing temperature control algorithms for thermal systems can be particularly challenging for several reasons. Firstly, most plants are composed of different control zones, each with its set of actuators and sensors, making them Multiple-Input Multiple-Output (MIMO) systems. Secondly, the derivation of accurate thermal systems models is impaired by the restrictive experimental design due to the long duration of the experiments. Most often, experimental data is scarce and is the result of trials of limited duration such as step responses. Consequently, simple First Order Lag Plus time Delay (FOLPD) Transfer Function (TF) models are commonly used to describe thermal systems, see e.g. Bai et al. (2008); He et al. (2014); Ryckaert et al. (1999); Zhang et al. (2014). Lastly, several, possibly conflicting, control specifications must be satisfied. The most common are setpoint tracking, disturbance rejection, and energy saving, but there are also application-oriented goals. For example, the temperature controllers of HVAC systems must ensure a suitable level of indoor thermal comfort and minimize building energy demand while rejecting disparate disturbances, stemming from the climate, occupant behavior, and electrical grid fluctuations (Serale et al. (2018)). In the food industry, convection ovens must reach a desired target temperature (setpoint tracking) in the shortest time possible and with negligible overshoots to meet food safety requirements and quality factors (Ryckaert et al. (1999)). Temperature uniformity within the oven cavity is also a concern. Environmental chambers share similar control specifications to convection ovens, although for different purposes (He et al. (2014)). Due to the limited complexity of the available models, control architectures based on Proportional-Integral-Derivative (PID) regulators are the most popular for thermal systems, see e.g. Bai et al. (2008); He et al. (2014); Ryckaert et al. (1999); Hu et al. (2018).

In this work, we focus on designing the temperature controllers for shrink tunnels, which are widely used in manufacturing applications for polymeric packaging. These machines are composed of an industrial convection oven and a conveyor belt that feeds products to it. The oven cavity is divided into multiple interconnected heating zones, each monitored by one or more thermocouples and with a dedicated set of heat resistors. Several convection fans favor air circulation inside the cavity. Before being inserted into the oven, the products are wrapped in a thin plastic film. The heat within the cavity shrinks the plastic and tightly envelopes the products, creating the packs. The heat resistors are connected to the electrical grid via relays, which modulate the voltages across them following the Pulse-Width Modulation (PWM) rationale. The temperature controller is responsible for producing the duty cycles of the just mentioned PWM signals. Several control specifications need to be met: (i) to maximize machine uptime, the air temperature inside the oven must reach a target temperature that is suited for the heat-shrinking process in the shortest time possible, (ii) deviations from the target temperature due to the insertion of products inside the cavity must be kept at a minimum to preserve the quality of the plastic wrapping, (iii) the downtime after machine shut down (e.g. due to possible issues on

the production line) must be mitigated by the regulator, and (iv) energy saving.

Contributions. In this paper, we focus on a shrink tunnel used in bottle packs manufacturing processes. Firstly, we derive a FOLPD model for the system under study based on experimental data. Then, we propose a model-based centralized control architecture that tackles the previously mentioned control specifications by combining several strategies from the control systems literature. The controller includes an inverted decoupler (Garrido et al. (2011)), a PI regulator for each heating zone, and a suitable Anti-Windup (AW) scheme. In particular, we extend the conditioned transfer AW algorithm in Peng et al. (1996), derived for Single Input Single Output (SISO) systems, to the MIMO case to address control actions limitations and mitigate the downtime after machine shut down. The control specifications are taken into account when calibrating the PI regulators via an ad hoc tuning rule. The performances of the proposed control architecture are experimentally validated on a shrink tunnel workbench.

Organization. The rest of this paper is organized as follows. Section 2 presents the shrink tunnel under study, whose model is described in Section 3. Then, Section 4 is devoted to the derivation of the control architecture. Its performances are experimentally validated in Section 5. Lastly, Section 6 gives some concluding remarks.

Notation. We denote by $\mathbb{C}$, $\mathbb{R}$, $\mathbb{Z}$, and $\mathbb{N}$ the set of complex, real, integer, and natural numbers respectively ($0 \notin \mathbb{N}$). Given $n, m \in \mathbb{N}$, $\mathbb{C}^n$ is the set of complex column vectors of dimension n while $\mathbb{C}^{n\times m}$ is the set of complex matrices of dimension $n \times m$. $I_n \in \mathbb{R}^{n\times n}$ is the $n \times n$ identity matrix, and $\operatorname{diag}\{a_1, \ldots, a_n\} \in \mathbb{R}^{n\times n}$ is the diagonal matrix with diagonal entries $a_1, \ldots, a_n \in \mathbb{R}$. $\mathbb{R}_{>0}$ and $\mathbb{R}_{\geq 0}$ stand for the set of positive and non-negative real numbers respectively. In what follows, $t \in \mathbb{R}$ denotes the time (in s) and $f(t), f : \mathbb{R} \to \mathbb{R}$, a continuous-time signal. Given a signal $f(t)$ such that $f(t) = 0, \forall t < 0$, $\mathcal{L}[f] : \mathbb{C} \to \mathbb{C}, F(s) = \mathcal{L}[f(t)]$, denotes the Laplace transform of $f(t)$ (Ogata (2010)). The same notation is used for vectors of signals, which are written in bold. Lastly, mod is the modulo operation.

2. SYSTEM DESCRIPTION

The schematic of the shrink tunnel under study is depicted in Fig. 1a and Fig. 1b, highlighting its main components. The industrial oven is 4.10 m long, 2.20 m tall and 1.40 m wide, while the conveyor belt is 5.70 m long. Before being inserted into the oven cavity, the bottles are mechanically grouped together and covered by a thin plastic film. An infrared sensor placed at the entrance of the oven detects when the beverages are being fed to it (see Fig. 1a). The heat shrinks the plastic and tightly envelopes the bottles, creating the packs. The oven cavity can house several bottles simultaneously and is divided into two interconnected heating zones. The heat in each zone is produced by a pair of heat resistors, located in separate compartments. The heat resistors are connected to the electrical grid via relays (one per pair of heat resistors, i.e. one per zone), which modulate the voltages across them. In particular, the relays are responsible for producing the voltage PWM signals based on the duty cycles supplied by a temperature controller. The hot air in the proximity of the heat resistors diffuses inside the oven cavity by means of four convection fans installed at the top of the oven. The air temperature inside the oven is measured by one thermocouple per zone.

We have at our disposal a workbench that can simulate a continuous supply of beverages via an additional conveyor belt that loops around the shrink tunnel (see Fig. 1c). The signals of interest for the shrink tunnel workbench under study are ($i \in \{1, 2\}$ denotes the zone of belonging):

- The temperatures $y_i(t) \in \mathbb{R}$ (in °C);
- The voltages across each pair of heat resistors $V_i(t) \in \mathbb{R}_{\geq 0}$ (in V), which are PWM signals with duty cycles $u_i(t) \in [0, 1]$;
- The heat flow rates $q_i(t) \in \mathbb{R}_{\geq 0}$ (in $\frac{\text{J}}{\text{s}}$) produced by the heat resistors pairs;
- The reading of the infrared sensor $d(t) \in \{0, 1\}$, which detects the presence ($d(t) = 1$) or absence ($d(t) = 0$) of bottle packs at the entrance of the oven.

The temperatures, voltages, duty cycles, and heat flow rates are grouped inside the vectors $\boldsymbol{y}(t) \in \mathbb{R}^2, \boldsymbol{V}(t) \in \mathbb{R}^2_{\geq 0}, \boldsymbol{u}(t) \in [0, 1]^2$, and $\boldsymbol{q}(t) \in \mathbb{R}^2_{\geq 0}$ respectively.

3. SHRINK TUNNEL MODELLING AND IDENTIFICATION

In this Section, we derive a control-oriented model for the shrink tunnel under study. Fig. 2 depicts the block diagram of the system. We assume that the overall temperatures within the oven cavity are the sum of three contributions: $\boldsymbol{y}'(t) \in \mathbb{R}^2$, $\boldsymbol{y}''(t) \in \mathbb{R}^2$, and $y'''(t) \in \mathbb{R}$, i.e.

$$\begin{aligned}\boldsymbol{Y}(s) &= \boldsymbol{Y}'(s) + \boldsymbol{Y}''(s) + [1\ 1]^\top \cdot Y'''(s) \\ &= \boldsymbol{G}(s) \cdot \boldsymbol{U}(s) + \boldsymbol{H}(s) \cdot D(s) + [1\ 1]^\top \cdot Y'''(s).\end{aligned} \tag{1}$$

The first term originates from the heat produced by the heat resistors (which depends on the duty cycles $\boldsymbol{u}(t)$), the second stems from the flow of bottle packs $d(t)$, the third one is the ambient temperature $y'''(t)$. In what follows, we derive a TF matrix $\boldsymbol{G}(s) \in \mathbb{C}^{2\times 2}$ describing the relationship between $\boldsymbol{u}(t)$ and $\boldsymbol{y}(t)$. The derivation of the TF matrix $\boldsymbol{H}(s) \in \mathbb{C}^2$ is out of scope of this paper.

Shrink tunnel modelling. The heat flow rates $q_i(t)$ produced by the heat resistor pairs depend on the square of the voltages across them $V_i(t)$ according to:

$$q_i(t) = R_{\text{heat}}^{-1} \cdot V_i(t)^2, \quad i \in \{1, 2\}, \tag{2}$$

where $R_{\text{heat}} \in \mathbb{R}_{>0}$ (in Ω) is the resistance of a pair of heat resistors. In particular, the voltages are PWM signals with duty cycles $u_i(t)$ and period $T_{\text{P}} \in \mathbb{R}_{>0}, T_{\text{P}} = 1\,\text{s}$. Let $k \in \mathbb{Z}$ be the PWM time interval index such that the k-th interval is defined as:

$$\mathcal{I}_k = \Big[k \cdot T_{\text{P}}, (k + 1) \cdot T_{\text{P}}\Big). \tag{3}$$

By definition, $u_i(t)$ are piecewise constant signals since

$$u_i(t) = u_i(k \cdot T_{\text{P}}), \quad \forall t \in \mathcal{I}_k, k \in \mathbb{Z}, \tag{4}$$

holds, i.e. the duty cycles cannot change during a PWM interval. The corresponding voltage signals read as:

$$V_i(t) = \begin{cases} V_{\text{g}} & \text{if } k \cdot T_{\text{P}} \leq t < [k + u_i(t)] \cdot T_{\text{P}} \\ 0 & \text{if } [k + u_i(t)] \cdot T_{\text{P}} \leq t < [k + 1] \cdot T_{\text{P}} \end{cases}, \tag{5}$$

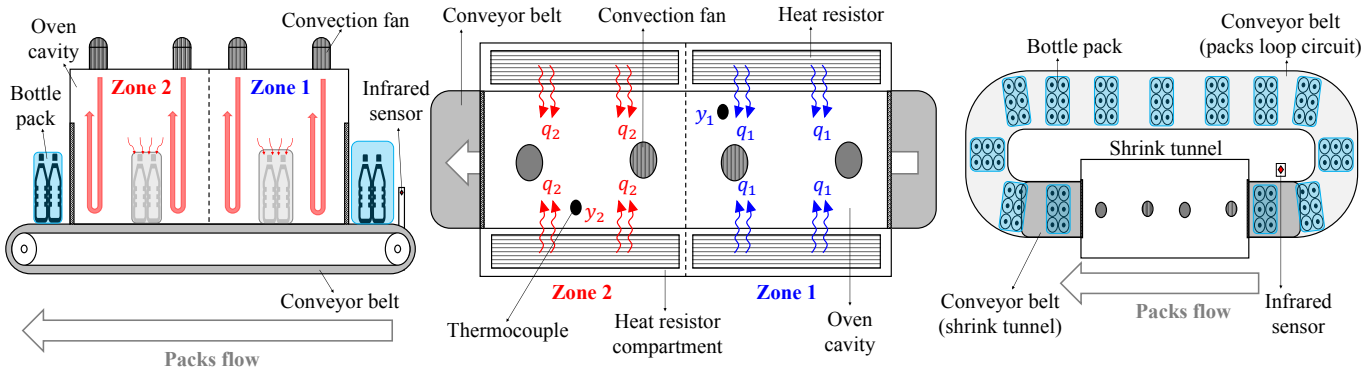

(a) – Shrink tunnel (front view). **(b) – Shrink tunnel (top view).** **(c) – Shrink tunnel workbench.**

Fig. 1. Schematic of the considered shrink tunnel and of the workbench at our disposal.

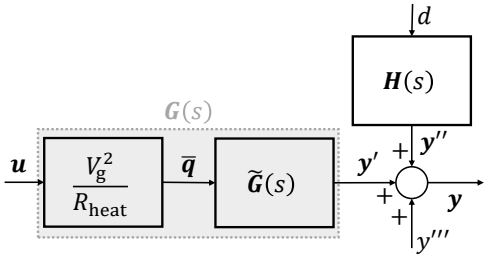

Fig. 2. Block diagram of the shrink tunnel under study.

where $V_\mathrm{g} \in \mathbb{R}_{>0}$ (in V) is the grid voltage, which is (roughly) constant during normal operation of the shrink tunnel. Given that the PWM period T_P (1 s) is notably smaller than the time constants associated with the heating and cooling dynamics (which are in the order of minutes) due to the high thermal inertia of the oven, we consider the average heat flow rates $\bar{q}_i(t)$ for each PWM interval rather than the instantaneous rates $q_i(t)$:

$$\begin{aligned}\bar{q}_i(t) &= \frac{1}{T_\mathrm{P}} \cdot \int_{k \cdot T_\mathrm{P}}^{(k+1)\cdot T_\mathrm{P}} q_i(\tau)\, d\tau, \quad \forall t \in \mathcal{I}_k, k \in \mathbb{Z} \\ &= R_\mathrm{heat}^{-1} \cdot V_\mathrm{g}^2 \cdot u_i(k \cdot T_\mathrm{P}) = R_\mathrm{heat}^{-1} \cdot V_\mathrm{g}^2 \cdot u_i(t). \quad (6)\end{aligned}$$

Adapting from the temperature control literature reviewed in Section 1, we model the relationship between the average heat flow rates $\bar{q}_j(t), j \in \{1,2\}$, and the temperatures $y_i'(t), i \in \{1,2\}$, using a FOLPD TF $\tilde{G}_{ij}(s) \in \mathbb{C}$:

$$Y_i'(s) = \tilde{G}_{ij}(s) \cdot \bar{Q}_j(s), \quad \tilde{G}_{ij}(s) = \frac{\tilde{\mu}_{ij}}{1 + s \cdot \tau_{ij}} \cdot e^{-s \cdot \gamma_{ij}},$$

where $\tilde{\mu}_{ij} \in \mathbb{R}_{>0}$ (in $\frac{^\circ\mathrm{C}\cdot\mathrm{s}}{\mathrm{J}}$) is the gain, $\tau_{ij} \in \mathbb{R}_{>0}$ (in s) is the time constant, and $\gamma_{ij} \in \mathbb{R}_{>0}$ (in s) is the time delay. Due to the linearity of the Laplace transform (Ogata (2010)) and (6), $\bar{Q}_j(s) = R_\mathrm{heat}^{-1} \cdot V_\mathrm{g}^2 \cdot U_j(s)$, leading to:

$$Y_i'(s) = G_{ij}(s) \cdot U_j(s), \quad G_{ij}(s) = \frac{\mu_{ij}}{1 + s \cdot \tau_{ij}} \cdot e^{-s \cdot \gamma_{ij}}, \quad (7)$$

where $\mu_{ij} = \tilde{\mu}_{ij} \cdot R_\mathrm{heat}^{-1} \cdot V_\mathrm{g}^2$ (in °C). Consequently, the TF matrix $\boldsymbol{G}(s)$ in (1) is given by:

$$\boldsymbol{G}(s) = \begin{bmatrix} G_{11}(s) & G_{12}(s) \\ G_{21}(s) & G_{22}(s) \end{bmatrix}. \quad (8)$$

Identification. The parameters of the TFs $G_{ij}(s), i,j \in \{1,2\}$, in (7) are estimated via open-loop experiments. Due to the long duration of the trials, we resort to two step response tests. In the first experiment, we set the duty cycle of the heat resistors in zone 1 to $u_1(t) = 0.6, \forall t \geq 0$, while the heat resistors of zone 2 are kept off (i.e. $u_2(t) = 0, \forall t \in \mathbb{R}$). Vice versa for the second experiment in which $u_1(t) = 0, \forall t \in \mathbb{R}$, and $u_2(t) = 0.6, \forall t \geq 0$. In both trials no bottle packs are inserted inside the oven. The ambient temperature is roughly constant, playing no role in the identification. We estimate $\mu_{ij}, \tau_{ij}, \gamma_{ij}$ for $G_{ij}(s), i,j \in \{1,2\}$, following the output-error approach (Verhaegen and Verdult (2007)). Table 1 reports the estimated parameters and the fits computed as $1-$NRMSE (Normalized Root Mean Square Error).

Table 1. Estimated parameters for the transfer functions $G_{ij}(s)$ in (7).

i	j	μ_{ij} [°C]	τ_{ij} [s]	γ_{ij} [s]	**Fit** [%]
1	1	192.3	841.7	110.9	95.3%
1	2	59.3	1315.9	162.4	95.1%
2	1	92.5	1218.4	133.1	96.5%
2	2	111.6	757.1	14.3	91.0%

4. CONTROL ARCHITECTURE

In this Section, we propose a control architecture for the shrink tunnel under study. The heat-shrinking process works as follows. The air temperature inside the oven must be kept at a desired value that allows the plastic film wrapped around the bottles to shrink uniformly during the pack travel time inside the cavity (see Fig. 1a). The target temperatures range from 120°C to 200°C, depending vastly on the installed plastic film, the processed beverages, and the airflow inside the oven cavity. In any case, the beverages are inserted inside the oven only when the target temperature is reached; any deviance from the desired temperature must be kept at a minimum during the heat-shrinking process to prevent quality degradation of the wrapping. Thus, the main control specifications are:

(S.1) The temperatures $y_i(t), i \in \{1,2\}$, must track piecewise constant setpoints $\mathrm{SP}_i(t) \in \mathbb{R}$ (in °C). When started from the ambient temperature, the $y_i(t)$'s must reach the target temperatures within 35 min. Instead, low-to-moderate setpoint changes ($10 \div 20$°C differences) must be handled within 20 min. This specification maximizes machine uptime.

(S.2) Disturbance rejection. Deviations from the target temperatures must be kept within a ±5°C tolerance

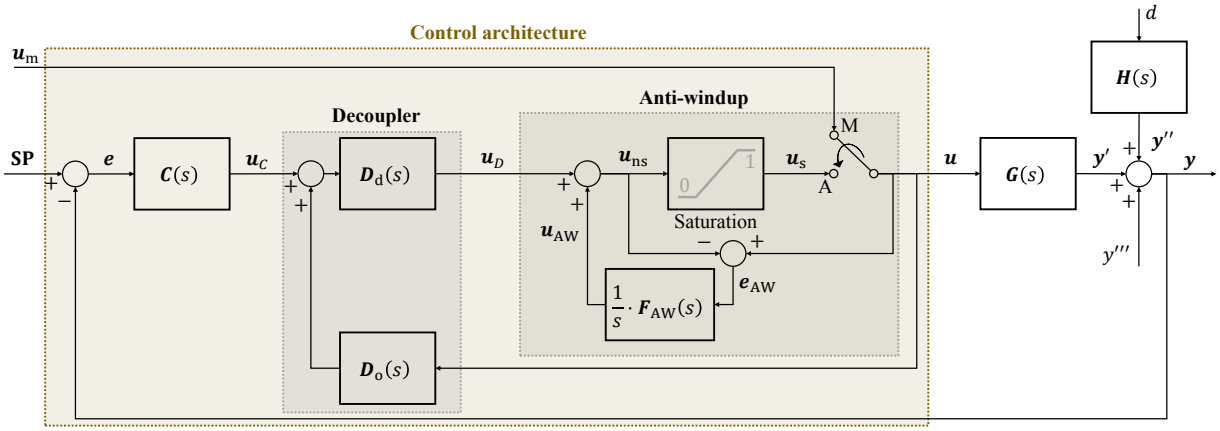

Fig. 3. Block diagram of the control architecture for the shrink tunnel under study.

during the heat-shrinking process. Failing to meet this specification for several minutes may impact the quality of the wrapping.

(S.3) The shrink tunnel is subject to several manual-automatic transitions during operation. Whenever there is any problem with the production line, the machine is shut down until it is solved. A shut down can be seen as switching the machine to manual mode by setting $u_i(t) = 0$ and $\mathrm{SP}_i(t) = 0°\mathrm{C}, i \in \{1,2\}$, temporarily. When the production line is restarted, the temperatures must converge to the setpoints in the shortest time possible, mitigating machine downtime.

(S.4) Energy saving. The controller should minimize the energy consumption of the heat resistors, which is given by (stemming from (4) and (5)):

$$\sum_{i=1}^{2}\int_0^{t_{\mathrm{end}}}\frac{V_i(\tau)^2}{R_{\mathrm{heat}}}d\tau=\sum_{i=1}^{2}\sum_{k=0}^{\frac{t_{\mathrm{end}}}{T_{\mathrm{P}}}-1}\frac{V_{\mathrm{g}}^2\cdot T_{\mathrm{P}}}{R_{\mathrm{heat}}}\cdot u_i(k\cdot T_{\mathrm{P}}), \quad (9)$$

where $t = 0$ is the time instant at which the shrink tunnel is turned on and $t = t_{\mathrm{end}}, t_{\mathrm{end}} \in \mathbb{R}_{>0}$, when it is stopped, assuming $t_{\mathrm{end}} \bmod T_{\mathrm{P}} = 0$.

(S.5) The control actions $u_i(t), i \in \{1,2\}$, must be between 0 and 1 (saturation).

Due to the MIMO nature of the shrink tunnel, we propose a centralized control architecture based on an inverted decoupler (Garrido et al. (2011)). The temperature in each zone is controlled by a PI regulator, whose tuning is eased by the presence of the decoupler and done according to (S.1) and (S.4). To minimize (9), the controller should produce smooth control actions. Disturbance rejection is intrinsically performed by the regulator, given its closed-loop nature. Thus, we will check experimentally (a-posteriori) if (S.2) is satisfied (see Section 5). The saturation of the duty cycles in (S.5) is handled via conditioned transfer anti-windup (Peng et al. (1996)), which also maximizes the setpoint tracking performances after manual-automatic transitions (covering (S.3) as well). The resulting control architecture is depicted in Fig. 3, where $\mathbf{SP}(t) = [\mathrm{SP}_1(t)\ \mathrm{SP}_2(t)]^\top \in \mathbb{R}^2$ is the setpoint vector, and $\boldsymbol{u}_{\mathrm{m}}(t) = [u_{\mathrm{m}_1}(t)\ u_{\mathrm{m}_2}(t)]^\top \in [0,1]^2$ are the manual control actions, see (S.3). In the control architecture, the saturation block works component-wise and as follows:

$$u_{\mathrm{s}_i}(t) = \max\left\{\min\left\{u_{\mathrm{ns}_i}(t), 1\right\}, 0\right\}, \quad i \in \{1,2\}. \quad (10)$$

$\boldsymbol{u}_{\mathrm{s}}(t) = [u_{\mathrm{s}_1}(t)\ u_{\mathrm{s}_2}(t)]^\top \in [0,1]^2$ are the limited control actions, while $\boldsymbol{u}_{\mathrm{ns}}(t) = [u_{\mathrm{ns}_1}(t)\ u_{\mathrm{ns}_2}(t)]^\top \in \mathbb{R}^2$ are those before saturation. The switch denotes which duty cycles should pass through in the block diagram when the system operates in Manual (M) or Automatic (A) mode.

Inverted decoupler. Consider the block diagram in Fig. 3. The decoupled control actions $\boldsymbol{u}_D(t) = [u_{D_1}(t)\ u_{D_2}(t)]^\top \in \mathbb{R}^2$ are given by:

$$\boldsymbol{U}_D(s) = \boldsymbol{D}_{\mathrm{d}}(s)\cdot[\boldsymbol{U}_C(s) + \boldsymbol{D}_{\mathrm{o}}(s)\cdot\boldsymbol{U}(s)], \quad (11)$$

where $\boldsymbol{u}_C(t) = [u_{C_1}(t)\ u_{C_2}(t)]^\top \in \mathbb{R}^2$ are the control actions produced by the PI regulators described by the TF matrix $\boldsymbol{C}(s) \in \mathbb{C}^{2\times 2}$. Let us assume that the system always operates in automatic mode and no saturations take place. Then, $\boldsymbol{u}(t) = \boldsymbol{u}_D(t)$ and (11) reduces to $\boldsymbol{U}_D(s) = \boldsymbol{D}_{\mathrm{inv}}(s)\cdot\boldsymbol{U}_C(s)$ with $\boldsymbol{D}_{\mathrm{inv}}(s) \in \mathbb{C}^{2\times 2}$,

$$\boldsymbol{D}_{\mathrm{inv}}(s) = [I_2 - \boldsymbol{D}_{\mathrm{d}}(s)\cdot\boldsymbol{D}_{\mathrm{o}}(s)]^{-1}\cdot\boldsymbol{D}_{\mathrm{d}}(s), \quad (12)$$

being the inverted decoupler TF matrix. By setting:

$$\boldsymbol{D}_{\mathrm{d}}(s) = I_2, \quad \boldsymbol{D}_{\mathrm{o}}(s) = \begin{bmatrix} 0 & -\frac{G_{12}(s)}{G_{11}(s)} \\ -\frac{G_{21}(s)}{G_{22}(s)} & 0 \end{bmatrix}, \quad (13)$$

it is possible to prove that the loop TF matrix $\boldsymbol{L}(s) \in \mathbb{C}^{2\times 2}$ amounts to (Garrido et al. (2011)):

$$\begin{aligned}\boldsymbol{L}(s) &= \boldsymbol{G}(s)\cdot\boldsymbol{D}_{\mathrm{inv}}(s)\cdot\boldsymbol{C}(s)\\ &= \mathrm{diag}\{G_{11}(s), G_{22}(s)\}\cdot\boldsymbol{C}(s).\end{aligned} \quad (14)$$

Given that, from a frequency response perspective, $\tau_{11} \approx \tau_{12}$ and $\tau_{22} \approx \tau_{21}$ (see Table 1), we can make the following approximations in (13):

$G_{12}(s)\cdot G_{11}(s)^{-1} \approx \mu_{12}\cdot\mu_{11}^{-1}, G_{21}(s)\cdot G_{22}(s)^{-1} \approx \mu_{21}\cdot\mu_{22}^{-1}$, resulting in a static decoupler.

PI controllers. Due to the centralized control architecture, we design a diagonal PI controller TF matrix:

$$\boldsymbol{C}(s) = \mathrm{diag}\{C_1(s), C_2(s)\},\ C_i(s) = \frac{K_{\mathrm{P}_i}}{T_{\mathrm{I}_i}}\cdot\frac{1+s\cdot T_{\mathrm{I}_i}}{s}, \quad (15)$$

where $K_{\mathrm{P}_i} \in \mathbb{R}$ (in $\frac{1}{°\mathrm{C}}$) and $T_{\mathrm{I}_i} \in \mathbb{R}$ (in s), $i \in \{1,2\}$, are the proportional gain and integral time constant respectively. Given that (14) holds approximately, when no saturations take place, under (15) the loop TF matrix

amounts to:

$$\boldsymbol{L}(s) \approx \text{diag}\{L_1(s), L_2(s)\}, \quad L_i(s) \approx G_{ii}(s) \cdot C_i(s). \quad (16)$$

Then, we can design each control loop independently, following traditional loop shaping rules (Ogata (2010)). We propose a simple model-based PI tuning rule to meet (S.1) and (S.4). By setting $T_{\text{I}_i} = \tau_{ii}$, the loop TFs in (16) amount to:

$$L_i(s) \approx K_{\text{P}_i} \cdot \frac{\mu_{ii}}{\tau_{ii}} \cdot \frac{1}{s} \cdot e^{-s \cdot \gamma_{ii}}.$$

We can easily derive the gain crossover frequency $\omega_{\text{c}_i} \in \mathbb{R}_{\geq 0}$ (in $\frac{\text{rad}}{\text{s}}$) and the phase margin $\varphi_{\text{m}_i} \in \mathbb{R}$ (in °) for each control loop (Ogata (2010)):

$$\omega_{\text{c}_i}(K_{\text{P}_i}) \approx K_{\text{P}_i} \cdot \frac{\mu_{ii}}{\tau_{ii}}, \quad (17a)$$

$$\varphi_{\text{m}_i}(K_{\text{P}_i}) \approx 90° - K_{\text{P}_i} \cdot \frac{180°}{\pi} \cdot \frac{\mu_{ii} \cdot \gamma_{ii}}{\tau_{ii}}, \quad (17b)$$

which depend linearly on K_{P_i}. (S.1) boils down to maximizing the gain crossover frequency since $\omega_{\text{c}_i}(K_{\text{P}_i})$ is an approximation of the frequency of the dominant pole of the closed-loop system (Ogata (2010)). Assuming that the system operates in the linear region (no saturations), the settling time of $y_i(t)$ after a step change in $\text{SP}_i(t)$ is roughly equal to (Ogata (2010)):

$$\sigma_i(K_{\text{P}_i}) \approx 4.6 \cdot \omega_{\text{c}_i}(K_{\text{P}_i})^{-1} \quad [\text{s}]. \quad (18)$$

We propose to tune the proportional gains K_{P_i} of the controllers by solving the following Linear Programs (LPs):

$$\arg\max_{K_{\text{P}_i}} \omega_{\text{c}_i}(K_{\text{P}_i}), \quad i \in \{1, 2\} \quad (19)$$
$$\text{s.t.} \quad \omega_{\text{c}_i}(K_{\text{P}_i}) \leq \omega_{\text{c}_{\max}}, \ \varphi_{\text{m}_i}(K_{\text{P}_i}) \geq \varphi_{\text{m}_{\min}}.$$

$\omega_{\text{c}_{\max}} \in \mathbb{R}_{\geq 0}$ (in $\frac{\text{rad}}{\text{s}}$) is a maximum gain crossover frequency that prevents unnecessary high K_{P_i}'s that can be chosen to meet (S.1) according to (18). For example, we could choose a minimum settling time $\sigma_{\min} \in \mathbb{R}_{>0}$ (in s) and set $\omega_{\text{c}_{\max}} = 4.6 \cdot \sigma_{\min}^{-1}$. Instead, $\varphi_{\text{m}_{\min}} \in [30°, 80°]$ is a minimum phase margin, set in a conservative range, which avoids excessive oscillations in $\boldsymbol{y}(t)$ and guarantees closed-loop stability of the system. High $\varphi_{\text{m}_{\min}}$ favor low PI gains, leading to smooth control actions and energy saving. In practice, the constraints in (19) are both upper bounds on K_{P_i}. Then, the solutions of the LPs in (19) are:

$$K_{\text{P}_i} = \min\left\{\omega_{\text{c}_{\max}} \cdot \frac{\tau_{ii}}{\mu_{ii}}, (90° - \varphi_{\text{m}_{\min}}) \cdot \frac{\pi}{180°} \cdot \frac{\tau_{ii}}{\mu_{ii} \cdot \gamma_{ii}}\right\}. \quad (20)$$

Anti-windup scheme. To tackle (S.3) and (S.5), we extend the conditioned transfer anti-windup algorithm described in Peng et al. (1996), which only covered the SISO case, to the proposed MIMO control architecture. In what follows, we sketch the proof demonstrating that, by choosing the AW TF matrix $\boldsymbol{F}_{\text{AW}}(s) \in \mathbb{C}^{2\times 2}$ as:

$$\boldsymbol{F}_{\text{AW}}(s) = \text{diag}\left\{T_{\text{I}_1}^{-1}, T_{\text{I}_2}^{-1}\right\}, \quad (21)$$

the tracking performances after manual-automatic transitions are maximized. In Fig. 3, $\boldsymbol{y}(t)$, $\boldsymbol{u}_{\text{ns}}(t)$, and $\boldsymbol{u}(t)$ are linked by:

$$\boldsymbol{Y}(s) = \mathbf{SP}(s) - \boldsymbol{W}(s) \cdot \boldsymbol{U}_{\text{ns}}(s) + \quad (22)$$
$$+ \boldsymbol{C}(s)^{-1} \cdot \boldsymbol{D}_{\text{d}}(s)^{-1} \cdot \left[\boldsymbol{D}_{\text{d}}(s) \cdot \boldsymbol{D}_{\text{o}}(s) + \frac{1}{s} \cdot \boldsymbol{F}_{\text{AW}}(s)\right] \cdot \boldsymbol{U}(s),$$
$$\boldsymbol{W}(s) = \boldsymbol{C}(s)^{-1} \cdot \boldsymbol{D}_{\text{d}}(s)^{-1} \cdot \left[I_2 + \frac{1}{s} \cdot \boldsymbol{F}_{\text{AW}}(s)\right].$$

We define the realizable reference vector $\mathbf{SPR}(t) \in \mathbb{R}^2$ as the setpoint vector such that if it had been applied instead of $\mathbf{SP}(t)$, the control actions before saturation, i.e. $\boldsymbol{u}_{\text{ns}}(t)$, would have been equal to the actual inputs $\boldsymbol{u}(t)$ obtained with the reference $\mathbf{SP}(t)$, without any saturation taking place. The same concept applies if manual control actions $\boldsymbol{u}_{\text{m}}(t)$ were applied instead of the ones computed by the controller. Analogously to the derivation in Peng et al. (1996) (this time in the MIMO case), by setting $\boldsymbol{u}(t) = \boldsymbol{u}_{\text{ns}}(t)$ in (22), we obtain the following expression for the realizable reference vector:

$$\mathbf{SPR}(s) = \boldsymbol{Y}(s) + \boldsymbol{C}(s)^{-1} \cdot \left[\boldsymbol{D}_{\text{d}}(s)^{-1} - \boldsymbol{D}_{\text{o}}(s)\right] \cdot \boldsymbol{U}(s). \quad (23)$$

Due to the definition of realizable reference, the outputs $\boldsymbol{y}(t)$ in (22) should match the outputs that we would obtain by applying $\mathbf{SPR}(t)$ in (23) instead of $\mathbf{SP}(t)$ (starting from the same initial conditions). Then, we can substitute $\boldsymbol{Y}(s)$ in (23) with (22), leading to:

$$\mathbf{SPR}(s) = \mathbf{SP}(s) + \boldsymbol{W}(s) \cdot [\boldsymbol{U}(s) - \boldsymbol{U}_{\text{ns}}(s)]. \quad (24)$$

By setting $\boldsymbol{F}_{\text{AW}}(s)$ as in (21), under (13) and (15), it is possible to prove that, in the time-domain, componentwise, (24) amounts to:

$$\text{SPR}_i(t) = \text{SP}_i(t) + {K_{\text{P}_i}}^{-1} \cdot [u_i(t) - u_{\text{ns}_i}(t)], \quad i \in \{1, 2\}.$$

Therefore, once $u_i(t) = u_{\text{ns}_i}(t)$, $\text{SPR}_i(t) = \text{SP}_i(t)$, and the setpoint tracking performances are maximized.

5. EXPERIMENTAL RESULTS

In this Section, the performances of the control architecture proposed in Section 4 are evaluated on the shrink tunnel workbench depicted in Fig. 1c. To do so, we discretize the TFs in (13), (15), and (21), and implement the corresponding lines of code in the software of the shrink tunnel microcontroller, which operates with the `C` programming language. Then, to analyze if each control specification is addressed, we carry out the following experiment. The shrink tunnel is turned on, starting from the ambient temperature, to assess the time required to reach a target temperature of 160°C (same for both zones). After that, several setpoint step changes are made, alternating between 150°C and 160°C, to analyze the tracking performances. We also include a brief machine shut down of roughly 5 minutes to evaluate the effectiveness of the implemented anti-windup strategy. Then, once the oven temperatures settle back at 160°C, the conveyor belt of the packs loop circuit is started, leading to the insertion of bottle packs inside the oven. After several minutes, the packs loop circuit is stopped to mimic the end of production.

To check if (S.1) and (S.3) are met, we compute the settling times during each setpoint tracking interval, which are defined as follows. Let $[t_{\text{A}}, t_{\text{B}}]$ be the time interval during which the setpoints are held constant at the value $\bar{\text{SP}}_{\text{AB}}$, i.e. $\text{SP}_1(t) = \text{SP}_2(t) = \bar{\text{SP}}_{\text{AB}}, \forall t \in [t_{\text{A}}, t_{\text{B}}]$. The settling time for the temperature $y_i(t), i \in \{1, 2\}$, is defined as:

$$\sigma_i = \min_{\tau \in [t_{\text{A}}, t_{\text{B}}]} \frac{1}{60} \cdot [\tau - t_{\text{A}}] \quad [\text{min}] \quad (25)$$
$$\text{s.t.} \left\{\left|\bar{\text{SP}}_{\text{AB}} - y_i(t)\right| \leq 0.02 \cdot \bar{\text{SP}}_{\text{AB}}, \forall t \geq \tau, t \in [t_{\text{A}}, t_{\text{B}}]\right\}.$$

Instead, for what concerns (S.2), we check if the deviations of $y_i(t)$ from $\text{SP}_i(t)$ are less than 5°C.

The PI controllers are tuned via (19) with $\varphi_{m_{min}} = 70°$ to minimize possible overshoots and/or temperature oscillations as well as favor energy saving, and $\omega_{c_{max}} = 5.1 \cdot 10^{-3} \frac{\text{rad}}{\text{s}}$, associated with a minimum settling time of $\sigma_{min} = 15\,\text{min}$, according to (S.1). Fig. 4 depicts the performances achieved by the proposed control architecture on the designed closed-loop experiment, highlighting the settling times $\sigma_i, i \in \{1, 2\}$, in (25) in each interval, and the deviations of $\boldsymbol{y}(t)$ from $\mathbf{SP}(t)$ when the packs are inserted into the oven. In any case, the σ_i's achieved by the proposed control architecture are well below the requirements imposed by (S.1). During machine shutdown, the temperatures lower rapidly: in 5 minutes, zone 2 loses roughly 30°C. Once the shrink tunnel goes back to automatic mode, the proposed anti-windup strategy drives the temperatures towards the setpoint of 150°C in the shortest time possible (less than 20 min), effectively tackling (S.3). For what concerns the disturbance rejection performances in (S.2), the controller is severely impaired by the limited heating power of the heat resistors installed on the shrink tunnel under study. We can clearly see that $u_2(t) = 1$ (upper limit) during production. Even in this unfavorable condition, the controller is able to meet the ±5°C tolerance for most of the trial, with deviances greater than 5°C for just a few minutes. In any case, notice the smoothness of the control actions, favoring energy saving in (S.4).

6. CONCLUSIONS

In this work, we design the temperature controller for a shrink tunnel used in bottle packs manufacturing processes. In particular, we develop a model-based control architecture starting from a FOLPD model of the system under study, estimated from open-loop experiments. The proposed control architecture addresses several demanding specifications: setpoint tracking, disturbance rejection, maximizing the tracking performances after manual-automatic transitions, energy saving, and actuator limitations. Each specification is satisfied by the proposed centralized controller, which includes an inverted decoupler, one PI regulator per heating zone, and an adequate anti-windup strategy, which is the extension of the conditioned transfer AW algorithm (Peng et al. (1996)) to the MIMO case. The derived control architecture is experimentally validated on the shrink tunnel workbench at our disposal, proving the overall satisfaction of each control specification thanks to an ad hoc tuning rule for the PI regulators. Future work is devoted to designing a feedforward controller to improve disturbance rejection performances.

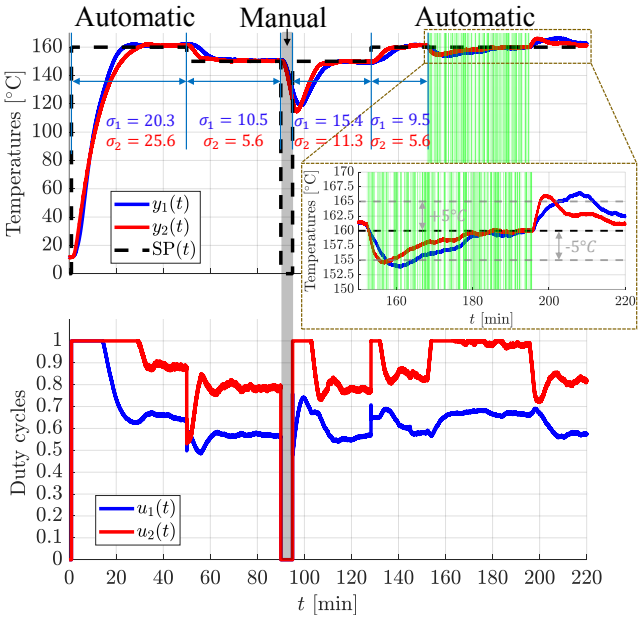

Fig. 4. Results achieved during the closed-loop experiment. The green vertical lines in the graph denote when $d(t) = 1$, i.e. when packs are inserted into the oven.

REFERENCES

Afroz, Z., Shafiullah, G., Urmee, T., and Higgins, G. (2018). Modeling techniques used in building hvac control systems: A review. *Renewable and sustainable energy reviews*, 83, 64–84.

Bai, J., Wang, S., and Zhang, X. (2008). Development of an adaptive smith predictor-based self-tuning pi controller for an hvac system in a test room. *Energy and Buildings*, 40(12), 2244–2252.

Garrido, J., Vázquez, F., and Morilla, F. (2011). An extended approach of inverted decoupling. *Journal of process control*, 21(1), 55–68.

He, W., Xu, G., and Shen, R. (2014). Control of temperature uniformity in the temperature chamber with centrifugal acceleration. *Journal of Process Control*, 24(12), 1–6.

Hu, Y., Tan, C., Broughton, J., Roach, P.A., and Varga, L. (2018). Nonlinear dynamic simulation and control of large-scale reheating furnace operations using a zone method based model. *Applied Thermal Engineering*, 135, 41–53.

Ogata, K. (2010). *Modern control engineering*, volume 5. Prentice hall Upper Saddle River, NJ.

Peng, Y., Vrancic, D., and Hanus, R. (1996). Anti-windup, bumpless, and conditioned transfer techniques for pid controllers. *IEEE Control systems magazine*, 16(4), 48–57.

Rastegarpour, S., Gros, S., and Ferrarini, L. (2020). Mpc approaches for modulating air-to-water heat pumps in radiant-floor buildings. *Control Engineering Practice*, 95, 104209.

Ryckaert, V.G., Claes, J.E., and Van Impe, J.F. (1999). Model-based temperature control in ovens. *Journal of Food Engineering*, 39(1), 47–58.

Serale, G., Fiorentini, M., Capozzoli, A., Bernardini, D., and Bemporad, A. (2018). Model predictive control (mpc) for enhancing building and hvac system energy efficiency: Problem formulation, applications and opportunities. *Energies*, 11(3), 631.

Vasičkaninová, A., Bakošová, M., Mészáros, A., and Klemeš, J.J. (2011). Neural network predictive control of a heat exchanger. *Applied Thermal Engineering*, 31(13), 2094–2100.

Verhaegen, M. and Verdult, V. (2007). *Filtering and system identification: a least squares approach*. Cambridge University Press.

Zhang, R., Xue, A., and Gao, F. (2014). Temperature control of industrial coke furnace using novel state space model predictive control. *IEEE transactions on industrial informatics*, 10(4), 2084–2092.